

Production of neutral and charged Higgs bosons of the MSSM at the future $e\gamma$ colliders

U. Cotti^{1,3}, J.L. Diaz-Cruz^{2*} and J.J. Toscano⁴

¹*SISSA-ISAS, via Beirut 2-4 I-34013, Trieste, Italy*

²*Instituto de Física, BUAP, A.P. J-48, 72570 Puebla, Pue. México*

³*Dpto. de Física, CINVESTAV-IPN, México D.F.*

⁴*Facultad de Ciencias Físico Matemáticas, BUAP, A. P. 1152, Puebla, Pue., México*

(June 14, 2021)

A complete study for the production of neutral ($h^0, H^0, A^0 (= \phi_i^0)$) and charged Higgs (H^\pm) bosons at electron-photon colliders is presented in the context of the minimal supersymmetric standard model. A particular choice of the non-linear R_ξ -gauge is used to evaluate the amplitudes of the reaction $e\gamma \rightarrow e\phi_i^0$. The resulting cross section indicates that it will be possible to detect a signal from the neutral Higgs bosons for most regions of parameter space at the future linear colliders with $\sqrt{s} = 500$ GeV through the reaction $e\gamma \rightarrow e\phi_i^0$. This reaction also offers the interesting possibility to measure the Higgs mass through the detection of the outgoing electron. The production of the charged Higgs boson (H^\pm) through the reaction $e\gamma \rightarrow \nu_e H^\pm$ has in general smaller values for the cross section, which seems more difficult to observe.

I. INTRODUCTION

The search for Higgs bosons at future colliders has become the focus of extensive studies, because of its importance as a test of the mechanism of electroweak symmetry breaking [1]. The detection of the full spectrum of scalars seems necessary in order to determine the nature of the physics that lies beyond the *standard model* (SM). Among the extensions of the SM, supersymmetry has received increasing attention, not only because of its aesthetical properties as a field theory, but also because the naturalness problem of the SM can be alleviated within the so-called *minimal supersymmetric standard model* (MSSM) [2].

The MSSM contains two Higgs doublets, whose physical spectrum includes a charged pair (H^\pm), two neutral CP-even scalars (h^0, H^0), and one pseudoscalar (A^0). The MSSM Higgs sector is determined at tree-level by two parameters, which are nowadays chosen as the A^0 mass and $\tan\beta$ (the ratio of the vevs. of the two Higgs doublets). This in turn fixes the values of the neutral Higgs mixing angle α and the remaining Higgs masses, which obey the tree-level relations, $m_{h^0} \leq m_Z \leq m_{H^0}$, $m_{h^0} \leq m_{A^0} \leq m_{H^0}$, $m_W \leq m_{H^\pm}$. However, these relations are substantially modified when the effect of radiative corrections is included [3–5]. In particular, it makes possible that $m_Z \leq m_{h^0}$, $m_{A^0} \leq m_{h^0}$, and for some regions of parameters m_{h^0} could even reach a value of about 130 GeV [6–8].

Current LEP2 limits on the Higgs masses are of about 90 GeV for the light scalar (h^0), and, depending on the value of $\tan\beta$, up to about 85 GeV for A^0 [9]. However LEP2 will be able to cover the region up to $m_{h^0} \lesssim 110$ GeV [10]. Recently, it was found that Tevatron can be used to test a significant portion of parameter space through the reaction $p\bar{p} \rightarrow Wh^0 + X$ [11], moreover the possibility to perform b-tagging with a high efficiency has opened the window to detect the mode $p\bar{p} \rightarrow b\bar{b}h^0 + X$ at LHC [12] and it will allow to test the large $\tan\beta$ region of parameters at Tevatron [13]. On the other hand, it has been shown [14] that LEP2 plus LHC results will be able to cover almost all the MSSM Higgs sector parameter space, and through a combination of the reactions $p\bar{p} \rightarrow t\bar{t} + h^0 (\rightarrow \gamma\gamma) + X$, $p\bar{p} \rightarrow h^0 (\rightarrow ZZ^*) + X$ [15–17] and weak boson fusion [18], the full region will be covered. At future linear colliders like NLC [19], TESLA [20] or JLC [21], it will be possible to search for neutral and charged Higgs bosons, through the production reactions $e^+e^- \rightarrow h^0 Z, h^0 \gamma$ [22,23] and $e^+e^- \rightarrow H^+H^-$ [24].

The future linear colliders can also operate in the $e\gamma$ mode [25]; in this case the production of the SM Higgs boson has been studied through the $\gamma\gamma \rightarrow \phi^0$ mechanism [26,27], and also with the full 1-loop two-body reaction $e\gamma \rightarrow \phi_i^0 e$ [28–30]. The production of the pseudoscalar Higgs boson A^0 through the reaction $e\gamma \rightarrow A^0 e$ has been studied too [31], using the photon pole approximation. Even though, these reactions can occur at tree-level, they receive the main contributions at one-loop level where the heavy particles of the model play an important role. These

*e-mail: ldiaz@sirio.ifuap.buap.mx

processes could be used to measure the couplings: $\phi^0\gamma^*\gamma$, $\phi^0Z^*\gamma$ [29,32,33], which constitute important one-loop predictions of the theory, and are also sensitive to the effects of new physics. Moreover, because of the possibility to measure the electron momenta, this reaction offers the possibility to determine the Higgs mass with high precision.

In this paper we present a detailed analysis of the production of the neutral and charged Higgs of the MSSM at γe^- colliders through the reactions $e\gamma \rightarrow e\phi_i^0$ ($\phi_i^0 = h^0, H^0, A^0$) and $e\gamma \rightarrow \nu H^\pm$, at the one-loop level. Our goal is to determine the regions of parameter space where a signal is detectable, and also to find out where it will be possible to distinguish between the MSSM and SM Higgs signals. We shall assume that the super-partners are heavy, and thus decouple from the amplitudes [34], however the effect of squarks will be included in the Higgs effective potential using the approximations presented in Ref. [35].

The organization of the paper is as follows: Section 2 discusses the production of neutral Higgs bosons. It includes a discussion of the region of parameter space that can be excluded, and also on the determination of the Higgs mass. Section 3 is devoted to the production of the charged Higgs, whereas the conclusions of our work are presented in Section 4. Details about the non-linear gauge used in the evaluation of the 1-loop amplitudes as well as the explicit formulae for the various amplitudes are presented in the Appendices.

II. THE NEUTRAL HIGGSSES

We now proceed to present the results of our calculation of the amplitudes of the reactions:

$$\gamma(k_1) + e^-(p_1) \rightarrow \phi^0(k_2) + e^-(p_2), \quad (1)$$

where ϕ^0 denotes any of h^0, H^0, A^0 , and we have also displayed the notation for incoming and outgoing momenta. We have organized the calculation according to the $U_{em}(1)$ gauge invariance, thus the diagrams are grouped as follows:

1. three-point diagrams characterized by the $\phi^0\gamma^*\gamma$ and by the $\phi^0Z^*\gamma$ coupling (Fig. 1-a) ;
2. Z and W-mediate box diagram and its related triangle graphs (Fig. 1-b,c,d),

The triangle graphs related to the Z- and W-mediated box diagrams are the one-loop $\phi^0 e^* e$ 3-point functions. These groups of diagrams are finite and gauge invariant by themselves. The group (1) receives contributions from loops of charged fermions, W gauge boson, and charged Higgs boson H^\pm . On the other hand, the group (2) is sensitive to the $\phi^0 W^+ W^-$ and $\phi^0 Z Z$ vertices, respectively. For A^0 there are contributions from fermionic triangles only, thus only group (1) appear.

In the linear gauge, the reaction $e\gamma \rightarrow e\phi_i^0$ receives also contributions coming from the reducible diagrams with the $Z^*\gamma$ self-energy, which is an extra complication because one needs to perform a renormalization of this term. However, in the nonlinear gauge this term is absent as consequence of the explicit $U_{em}(1)$ gauge symmetry in the W, goldstone and ghost sectors. Notice that there are no contributions coming from the charged Higgs boson to the group (2). This happens because we use the approximation $m_e = 0$ and also because there is no $\gamma W^\pm H^\pm$ vertex at tree-level.¹

A. Production of h^0, H^0

The Mandelstam variables used in this calculation are defined by $s = (k_1 + p_1)^2$, $t = (k_1 - k_2)^2$, and $u = (k_1 - p_2)^2$. In addition, $\epsilon^\mu(k_1, \lambda_1)$ will denote the γ polarization vector. We have evaluated the amplitudes using dimensional regularization, with the help of the program FeynCalc [36] and the numerical libraries FF [37,38].

The result for the total amplitude of the reaction $e\gamma \rightarrow e h^0(H^0)$ can be written as:

$$\mathcal{M} = \mathcal{M}_\gamma + \mathcal{M}_Z + \mathcal{M}_Z^{\text{box}} + \mathcal{M}_W^{\text{box}}, \quad (2)$$

where \mathcal{M}_γ , \mathcal{M}_Z , $\mathcal{M}_Z^{\text{box}}$, and $\mathcal{M}_W^{\text{box}}$ correspond to the sets of diagrams (1), (2), (3), and (4), respectively. The amplitudes coming from the $\phi^0\gamma^*\gamma$ and $\phi^0Z^*\gamma$ couplings can be written as follows:

¹We could think on possible contributions arising from reducible diagrams that include the $\gamma^*\phi^0$ and $Z^*\phi^0$ self-energies (with the virtual fields tied to the electronic line). However, it can be shown that these terms always vanish.

$$\mathcal{M}_{\gamma,Z} = \frac{i\alpha^2 m_W}{4s_w^3 c_w^4} \bar{u}(p_2) \gamma^\nu (a_{\gamma,Z} - b_{\gamma,Z} \gamma_5) u(p_1) \epsilon^\mu(k_1, \lambda_1) F_{\gamma,Z}(k_1 \cdot k_2 g_{\mu\nu} - k_{2\mu} k_{1\nu}), \quad (3)$$

where

$$F_\gamma = \frac{4s_w^2 c_w^4}{m_W^2 t} \left(\sum_f 2f_\phi N_c Q_f^2 F_f^{1/2} + v_\phi F_\gamma^1 + s_\phi F^0 \right), \quad (4)$$

$$F_Z = \frac{c_w^4}{m_W^2 (m_Z^2 - t)} \left(- \sum_f \frac{f_\phi C_V^f N_c Q_f}{c_w^2} F_f^{1/2} + v_\phi F_Z^1 - \frac{s_\phi c_{2w}}{2c_w^2} F^0 \right), \quad (5)$$

with $a_\gamma = 1$, $b_\gamma = 0$, $a_Z = 1 - 4s_w^2$, $b_Z = 1$, $t_w = \frac{s_w}{c_w}$, and $c_{2w} = c_w^2 - s_w^2$. The coefficients f_ϕ , v_ϕ , and s_ϕ characterize the $\phi^0 \bar{f}f$, $\phi^0 ZZ$, and $\phi^0 H^\pm H^\mp$ couplings in the MSSM, and are given by:

$$f_\phi = \begin{cases} \frac{\sin \alpha}{\sin \beta}, & H^0 \bar{u}u \\ \frac{\cos \alpha}{\cos \beta}, & H^0 \bar{d}d \\ \frac{\cos \alpha}{\sin \beta}, & h^0 \bar{u}u \\ -\frac{\sin \alpha}{\cos \beta}, & h^0 \bar{d}d, \end{cases}$$

$$v_\phi = \begin{cases} \cos(\beta - \alpha), & \phi^0 = H^0 \\ \sin(\beta - \alpha), & \phi^0 = h^0, \end{cases}$$

$$s_\phi = \begin{cases} \cos(\beta - \alpha) - \frac{1}{2c_w^2} \cos 2\beta \cos(\beta + \alpha), & \phi^0 = H^0 \\ \sin(\beta - \alpha) + \frac{1}{2c_w^2} \cos 2\beta \sin(\beta + \alpha), & \phi^0 = h^0. \end{cases}$$

The functions $F_f^{1/2}$, F^0 , F_γ^1 and F_Z^1 arising from fermion, scalar and gauge boson loops are given in the Appendix B.

The amplitude for the contributions of the Z -mediated box diagram, including the related $\phi^0 e^* e^-$ triangle graphs, is the following:

$$\begin{aligned} \mathcal{M}_Z^{\text{box}} &= \frac{i\alpha^2 m_W}{4s_w^3 c_w^4} \bar{u}(p_2) \gamma^\nu (a_Z - \gamma_5)^2 u(p_1) \epsilon^\mu(k_1, \lambda_1) \\ &\times [-A(t, s, u)(k_1 \cdot p_1 g_{\mu\nu} - p_{1\mu} k_{1\nu}) + A(t, u, s)(k_1 \cdot p_2 g_{\mu\nu} - p_{2\mu} k_{1\nu})], \end{aligned} \quad (6)$$

where the functions $A(t, s, u)$ and $A(t, u, s)$ are presented in the Appendix B.

The amplitude for the W -mediated box diagrams and its related triangle graphs is given by:

$$\begin{aligned} \mathcal{M}_W^{\text{box}} &= \frac{i\alpha^2 m_W}{4s_w^3 c_w^4} \bar{u}(p_2) \gamma^\nu (1 - \gamma_5)^2 u(p_1) \epsilon^\mu(k_1, \lambda_1) \{A_{12}(t, s, u) \\ &\times (k_1 \cdot p_1 g_{\mu\nu} - p_{1\mu} k_{1\nu}) - A_{21}(t, s, u)(k_1 \cdot p_2 g_{\mu\nu} - p_{2\mu} k_{1\nu})\}, \end{aligned} \quad (7)$$

where the functions A_i and A_{ij} are given in the Appendix B.

After squaring the total amplitude, the corresponding cross-section for this process is given by:

$$\hat{\sigma} = \frac{1}{16\pi s^2} \int_{m_\phi^2 - s}^0 dt |\overline{\mathcal{M}}|^2, \quad (8)$$

where

$$|\overline{\mathcal{M}}|^2 = \frac{\alpha^4 m_W^2}{64s_w^6 c_w^8} (-t) [(s^2 + u^2) F_{\gamma Z} + s^2 F_s + u^2 F_u], \quad (9)$$

with

$$F_{\gamma Z} = |F_\gamma|^2 + a|F_Z|^2 + 2a_Z \text{Re} (F_Z F_\gamma^*), \quad (10)$$

$$F_s = |A_{12}(t, s, u)|^2 + c|A(t, s, u)|^2 + 2\text{Re} \{ [A_{12}(t, s, u) - 2aA(t, s, u)] F_\gamma^* + [4bA_{12}(t, s, u) - 2dA(t, s, u)] F_Z^* - 2A_{12}(t, s, u) A^*(t, s, u) \}, \quad (11)$$

$$F_u = F_s(s \leftrightarrow u), \quad (12)$$

where we have defined $a = 1 + a_z^2$, $b = 1 + a_z$, $c = 1 + 6a_z^2 + a_z^4$, and $d = a_z(a_z^2 + 3)$.

Finally, in order to obtain the total cross-section (σ_T), one needs to convolute $\hat{\sigma}$ with the photon distribution, namely:

$$\sigma_T = \frac{1}{S} \int_{m_\phi^2}^{0.83S} f_\gamma\left(\frac{s}{S}\right) \hat{\sigma}(s) ds, \quad (13)$$

where S denotes the squared c.m. energy of the e^+e^- -system, and the photon distribution is given by:

$$f_\gamma = \frac{1}{D(\xi)} \left[1 - x + \frac{1}{1-x} - \frac{4x}{\xi(1-x)} + \frac{4x^2}{\xi^2(1-x)^2} \right], \quad (14)$$

where

$$D(\xi) = \left(1 - \frac{4}{\xi} - \frac{8}{\xi^2} \right) \log(1 + \xi) + \frac{1}{2} + \frac{8}{\xi} - \frac{1}{2(1 + \xi)^2}. \quad (15)$$

Notice that, as in Ref. [29], one should use, instead of the photon distribution, an exactly monochromatic initial photon beam which can help in distinguish the physical effects related to the particular collision process from details depending on the final realization of the laser beam.

To evaluate the cross-section for h^0 and H^0 , we have taken $m_t = 175$ GeV, and the values for the electroweak parameters given in the table of particle properties [39]. In fact, as it was discussed in Ref. [29], the contributions of the boxes can be neglected. The cross section for h^0 is about 4.2 fb for $m_{A^0} > 200$ GeV and $E_{c.m.} = 500$ GeV, as can be seen from Fig. 2. With the expected luminosity at the future linear colliders [19–21] of about $50 \text{ fb}^{-1}/\text{yr}$, it will be possible to observe up to about 210 $h^0 + e$ events, which should allow to study the properties of the Higgs boson. Among them, it will be interesting to test its spin and CP-even nature by studying the angular distributions, however this aspect is beyond the goal of the present work, where we are mainly interested in determining if the MSSM Higgs sector can be tested at electron-photon colliders. Total cross-sections for the production of the heavy Higgs boson H^0 as a function of the pseudoscalar mass m_{A^0} and for different values of $\tan\beta$ are shown in Fig. 3. These graphs present the total cross-section as a function of the pseudoscalar mass (m_{A^0}) for several values of $\tan\beta$ for c.m. energy of 500 GeV.

B. Production of A^0

On the other hand the amplitude for the production of the pseudoscalar contains only contributions from the fermionic triangles. Thus, the amplitude takes the form:

$$\mathcal{M} = \mathcal{M}_\gamma + \mathcal{M}_Z, \quad (16)$$

where

$$\mathcal{M}_\gamma = \frac{-i\alpha^2 Q_f^2 N_C f_\beta m_W}{s_w} \bar{u}(p_2) \gamma^\nu u(p_1) \epsilon^\mu(k_1, \lambda_1) \frac{4m_f^2}{m_W^2} C_0(t, m_A^2, m_f^2) \left(\frac{\epsilon_{\mu\nu\alpha\beta} k_1^\alpha k_2^\beta}{t} \right), \quad (17)$$

and

$$\mathcal{M}_Z = \frac{i\alpha^2 Q_f C_V^f N_C f_\beta m_W}{4s_w^3 c_w^2} \bar{u}(p_2) \gamma^\nu (C_V^e - C_A^e \gamma_5) u(p_1) \epsilon^\mu(k_1, \lambda_1) \frac{4m_f^2}{m_W^2} C_0(t, m_A^2, m_f^2) \left(\frac{\epsilon_{\mu\nu\alpha\beta} k_1^\alpha k_2^\beta}{t - m_Z^2} \right), \quad (18)$$

with $C_0(t, m_A^2, m_f^2) = C_0(t, m_A^2, 0, m_f^2, m_f^2, m_f^2)$ the Passarino-Veltman three-point scalar function written in the notation of the FeynCalc program and

$$f_\beta = \begin{cases} \cot \beta, & f = u \\ \tan \beta, & f = d, \end{cases} \quad (19)$$

The total squared amplitude is

$$|\overline{\mathcal{M}}|^2 = \frac{\alpha^4 Q_f^4 N_C^2 f_\beta^2}{s_w^2} \frac{-t}{m_A} \frac{s^2 + u^2}{t^2} \left[1 - \frac{C_V^e C_V^f}{2s_w^2 c_w^2 Q_f} \frac{t}{t - m_Z^2} \right] \quad (20)$$

$$+ C_V^{f^2} \frac{C_V^e{}^2 + C_V^f{}^2}{16s_w^4 c_w^4 Q_f^2} \left(\frac{t}{t - m_Z^2} \right)^2 \left[2m_f^2 C_0(t, m_A^2, m_f^2) \right]^2. \quad (21)$$

To obtain the total cross-section we use the expressions written previously for the CP-even Higgs bosons (Eqs. 13-15). Results are shown in Fig. 4, where we plot again the total cross-section as a function of the pseudoscalar mass (m_{A^0}), for several values of $\tan \beta$ and for c.m. energy of 500 GeV. It can be noted that the cross-section for A^0 is smaller than the one resulting for h^0/H^0 . Thus, in this case it will be more difficult to detect the signal.

C. Backgrounds and exclusion contours

The final signature for the reaction $e\gamma \rightarrow e\phi_i^0$ depends on the decay of the Higgs boson. For h^0 , the dominant mode is into $b\bar{b}$, whereas for H^0 and A^0 this decay can also be relevant for some regions of parameter space. To evaluate the B.R. of the Higgs bosons we shall assume that the decays into SUSY modes (i.e. charginos, neutralinos, sfermions) are not allowed and take the relevant equation for the decay widths from [1]. Our results are in agreement with the ones obtained in the literature, for instance in ref. [40]. Thus, we shall concentrate on the signature coming from the decay $\phi_i^0 \rightarrow b\bar{b}$. In this case the main background comes from $e\gamma \rightarrow eb\bar{b}$, which receives contribution from 8 graphs at tree level; we have evaluated numerically this processes using CompHep [41,42]. Following Dicus et al. [31], we have also imposed a cut on the angular distribution of the outgoing electron ($|\cos \theta| < 0.98$, relative to the incident photon) that reduces significantly the background, while retaining most of the signal rate. To determine the region of parameter space, which is taken as the plane $\tan \beta - m_{A^0}$, where the Higgs signal is detectable, we have proceeded as follows: for each value of m_{A^0} we evaluate the Higgs masses and the cross-sections, then we find the value for $\tan \beta$ where the cross-section of the signal is above the background at the 3 and 5 σ level.

In Fig. 5, we show the regions in the plane $\tan \beta - m_{A^0}$ where the cross-section coming from h^0 has detectable values. The region to the right from the heavy line is where the signal is detectable, above backgrounds at the 3 σ level. The dashed line denotes the contour at the 5 σ level. It can be seen that the signal is above the backgrounds for a significant region of parameter space.

On the other hand, Fig. 6 shows the region where the cross-section from H^0 reaches detectable values. Again, The region to the left from the heavy (dashed) line is where the signal is detectable at the 3 (5) σ level. It can be noticed that this region covers the sector of parameter space where it is more difficult to detect the light h^0 . Thus, the cross-sections for h^0/A^0 and H^0/A^0 play a complementary role in providing a detectable signal for the full parameter space. Moreover, we also notice from the superposition of Figs. 5 and 6, that there is a small region where the two Higgs boson signals can be detected, which will allow to distinguish clearly between the MSSM and the SM Higgs sectors.

Finally, we also want to stress the fact that this reaction offers a unique opportunity to obtain a clean measurement of the Higgs mass, thanks to the possibility to measure the outgoing electron momentum. The mass of the Higgs boson is related to the maximal energy of the electron as:

$$m_{h^0} = \sqrt{s} - E_{max}. \quad (22)$$

Thus, the precision attained for the electron energy will translate into a good determination of the Higgs mass.

On the other hand, the largest values of the cross-section for A^0 are obtained for large values of $\tan \beta$ (which is usually assumed to be at most of order 50); however, we find that even in this case the resulting cross-section does not seem to give a detectable signal. Moreover, for large values of $\tan \beta$ there appears a mass-degeneracy between A^0 and h^0 or H^0 , which will make difficult to distinguish the individual signals. In this case, it will be necessary to optimize the cuts to be able to detect the pseudoscalar A^0 , and to separate it from the largest signals coming from h^0 and H^0 . Otherwise, one would have to add the respective signals; for instance, one could imposed the criteria that

whenever the difference between the Higgs masses is less than 5 GeV (a conservative criteria given the possibility to obtain a precise measurement of the Higgs mass), the individual contributions to the signal must be combined. We find that this only helps to enlarge the exclusion contours for $\tan\beta$ above 30.

Another option to detect A^0 (and a heavy H^0 too) is to use the planned second and third stages of the future e-gamma colliders [19–21], which could reach an energy of 1 TeV and 2 TeV, with integrated luminosities that could reach 125 and 500 fb^{-1} , respectively.

III. THE CHARGED HIGGS

Now, turning to the production of the charged Higgs, we observe that it can also proceed through the 1-loop reaction:

$$\gamma(k_1) + e^-(p_1) \rightarrow H^-(k_2) + \nu_e(p_2). \quad (23)$$

The diagrams encountered in the calculation of the $e^-\gamma \rightarrow \nu H^-$ are shown in Fig. 8. They include: triangle graphs with bosons and fermions in the loop (Fig. 8a), seagull-type graphs with bosonic contributions (Fig. 8b-c), and finally those with self-energy insertions (Fig. 8d, 8e, 8f). Fig. 8f gives a vanishing contribution for massless external fermions.

A. Production of H^\pm

Our result for the total amplitude is written as:

$$\begin{aligned} \mathcal{M} = & \frac{i\alpha^2}{2\sqrt{2}s_w^3 m_W(t - m_W^2)} \bar{u}(p_2)\gamma^\nu(1 - \gamma_5)u(p_1)\epsilon^\mu(k_1, \lambda_1) \\ & \times \left[(V_f + V_{H^+\phi^0} + V_{W\phi^0}) (k_{2\mu}k_{1\nu} - g_{\mu\nu}k_1 \cdot k_2) + iA_f\epsilon_{\mu\nu\alpha\beta}k_1^\alpha k_2^\beta \right] \end{aligned} \quad (24)$$

where V_f , $V_{H^+\phi^0}$, $V_{W\phi^0}$ and A_f denote the contribution from the different sets of graphs shown in Fig. 8 and are given in the Appendix C.

Fig. 9 shows the cross-section for our process for several values of $\tan\beta$ ($= 1.5, 5, 10$). The cross section is small, about 0.5 fb for $m_{H^\pm} = 200$ GeV and $E_{c.m.} = 500$ GeV, which can give 25 events with an expected future linear colliders luminosities of 50 fb^{-1}/yr . In Fig. 10 we compare the cross section from $e\gamma \rightarrow H^-\nu$, with the pair production $e^+e^- \rightarrow H^+H^-$, $e\gamma \rightarrow H^+H^-e$ and $\gamma\gamma \rightarrow H^+H^-$. The production mechanisms $e^+e^- \rightarrow H^+H^-$, $\gamma\gamma \rightarrow H^+H^-$, have been discussed in the literature [43]. On the other hand, the reaction $e\gamma \rightarrow H^+H^-e$ is evaluated using the Williams-Weizsacker approximation (for the second photon) and we use the sub-reaction $\gamma\gamma \rightarrow H^+H^-$. It can be seen that the single production dominates only for large Higgs masses i.e. for values that lay beyond the threshold for pair production.

B. Backgrounds

In this paper we only show (Fig. 9) the results for fixed values of $\tan\beta = 1.5, 5, 10$, and as can be appreciated it turns out that the resulting cross-section has smaller results, which hardly seem detectable. In order to determine if the signal is detectable, one needs to consider the potential backgrounds, which depend on the Higgs mass, since this determines the decay signatures. For instance, if $m_{H^\pm} < m_t + m_b$, the dominant decay mode is $H^\pm \rightarrow \tau\nu$ which reaches a branching ratio of order 1 for most values of $\tan\beta$. In this case the background will come from the production $\gamma e \rightarrow W^*\nu$, which for masses $m_{H^\pm} \approx m_W$ will be much larger than the signal (it reaches $\sigma \simeq 4pb$) and probably will not allow detection. For masses somehow larger, both the signal and the background will be more suppressed and the question of detectability will depend on the experimental ability to identify the decay mode and to reconstruct the charged Higgs mass.

For heavier Higgs masses, $M_{H^\pm} > m_t + m_b$, the dominant Higgs decay is into $t + \bar{b}$, and in this case one needs to compare the signal with the background arising from single top production, $e\gamma \rightarrow \nu t\bar{b}$ for $M_{H^\pm} > m_t + m_b$, which according to the results of Boos et al. [44], has $\sigma \simeq 15fb$ for $\sqrt{s} = 500$ GeV and $m_t = 175GeV$. Thus we can see that at the level of total cross-section the background is again larger than the signal. However if one makes a cut in the invariant mass of the $t - b$ system, then it will be possible to reduce the background.

IV. CONCLUSIONS

We have studied the production of the neutral CP-even and charged Higgs boson of the MSSM (h^0, H^0, H^\pm) at future $e\gamma$ colliders, through the reactions $e\gamma \rightarrow eh^0, eH^0, eA^0, \nu H^-$. The amplitudes are evaluated using a non-linear R_ξ -gauge, which greatly simplifies the calculation. The resulting cross section indicates that it is possible to detect the light neutral Higgs boson (h^0) for most values of parameters. On the other hand, detection of the heavy neutral Higgs bosons H^0 seems possible only for light values of m_{A^0} . We have determined the regions in the plane $\tan\beta - m_{A^0}$ where the signal is above the backgrounds. The cross-sections for h^0 and H^0 play a complementary role, since the region where H^0 reaches detectable values occurs precisely in the region where it is more difficult to detect the light h^0 . Thus, both reactions allow to cover the full plane $\tan\beta - m_{A^0}$ with at least one detectable signal. However, it is found that the possibility to distinguish the MSSM from the SM case, through detection of both h^0 and H^0 signals, occurs only for a limited region of parameter space.

On the other hand, the results for the pseudoscalar and the charged Higgs boson have smaller values of the cross-section, which seems difficult to detect.

ACKNOWLEDGMENTS

We acknowledge financial support from CONACYT and SNI (México). U.C. wish to acknowledge useful discussions with Borut Bajc and Goran Senjanović.

APPENDIX A: THE NON-LINEAR GAUGE

In the evaluation of the above processes, we have used a Feynman-t'Hooft version of the nonlinear gauge [45–49] that greatly simplify the calculation. In order to appreciate the advantages that offer a nonlinear gauge, we find convenient to compare it with the conventional linear gauge for the SM. It is well known that in a linear gauge only the charged fermion sector presents explicit electromagnetic gauge symmetry ($U_{em}(1)$), since the gauge fixing procedure used for the $SU(2)$ sector destroys manifest $U_{em}(1)$ symmetry in the charged gauge boson (W^\pm) and ghosts sectors (c, \bar{c}), when they are considered separately, because the gauge functional used to define the W -propagator does not transform covariantly under the $U_{em}(1)$ symmetry. It follows that instead of obeying naive Ward identities, these sectors are related through Ward-Slavnov identities. In order to obtain a finite and $U_{em}(1)$ -invariant result for higher-order (loop) calculations, one must sum over the contributions arising from the W gauge boson, the charged ghosts, and the $W^\pm G^\mp$ combined effects, G^\pm denotes the would-be Goldstone boson. On the other hand, the functional used to define the W -propagator in the non-linear gauge contains the electromagnetic covariant derivative. Thus, the $U_{em}(1)$ symmetry is respected by each charged sector of the SM. It follows that a finite and $U_{em}(1)$ gauge invariant result is obtained for each type of diagram containing a given kind of charged particles. Moreover, the number of diagrams involved is considerably reduced because there are no $W^\pm G^\mp$ combined effects. In the SM, the functionals that define the W , Z , and γ propagators are given by:

$$\begin{aligned} f^+ &= \bar{D}_\mu W^{+\mu} - i\xi m_W G^+, \\ f^Z &= \partial_\mu Z^\mu - \xi m_Z G^0, \\ f^A &= \partial_\mu A^\mu, \end{aligned} \tag{A1}$$

where $D_\mu = \partial_\mu - ig'B_\mu$, with $B_\mu = -s_w Z_\mu + c_w A_\mu$, G^0 is the neutral would-be Goldstone. ξ is the gauge parameter, which in general is different for each of the three gauge bosons. However, in the non-linear Feynman-t'Hooft version of this gauge, one takes $\xi = 1$ for all sectors. The gauge fixing Lagrangian is given by:

$$\mathcal{L}_{GF} = -\frac{1}{\xi} f^+ f^- - \frac{1}{2\xi} (f^Z)^2 - \frac{1}{2\xi} (f^A)^2, \tag{A2}$$

which in turn removes the $W^\pm G^\mp \gamma$ and $W^\pm G^\mp Z$ vertices from the Higgs kinetic energy term. Notice that the $f^+ f^-$ term is $U_{em}(1)$ gauge invariant, which implies that the Fadeev-Popov \mathcal{L}_{FP} Lagrangian is also $U_{em}(1)$ -invariant. It is also possible to proceed further with this scheme and remove more un-physical vertices, such as $\phi^0 W^\pm G^\mp \gamma(Z)$ and $G^0 W^\pm G^\mp \gamma(Z)$. This procedure requires to define the functionals f^\pm nonlinearly both in the vector and scalar parts. However, for the present purposes it is sufficient to use the scheme presented above.

In this case only the couplings in the gauge and ghost sectors are modified. We shall give the lagrangian for these sectors in a form that clarifies the role of the electromagnetic gauge invariance. For this, we define the derivative:

$\hat{D}_\mu = \partial_\mu - igW_\mu^3$, with $W_\mu^3 = c_w Z_\mu + s_w A_\mu$. This operator shares with the derivative D defined above the property of containing the e.m. covariant derivative. After adding the gauge-fixing lagrangian, one obtains the couplings for the gauge bosons (W, Z, A), which are contained in:

$$\begin{aligned}\mathcal{L} = & -\frac{1}{2}(\hat{D}_\mu W_\nu^+ - \hat{D}_\nu W_\mu^+)^\dagger (\hat{D}^\mu W^{+\nu} - \hat{D}^\nu W^{+\mu}) - ig(s_w F_{\mu\nu} + c_w Z_{\mu\nu})W^{-\mu}W^{+\nu} \\ & -ig\left[s_w F_{\mu\nu} + c_w Z_{\mu\nu} + i\frac{g}{2}(W_\mu^- W_\nu^+ - W_\nu^- W_\mu^+)\right]W^{-\mu}W^{+\nu} \\ & -\frac{1}{\xi}(\bar{D}_\mu W^{+\mu})(\bar{D}_\nu W^{+\nu})^\dagger + m_W^2 W_\mu^- W^{+\mu} \\ & -\frac{1}{4}Z_{\mu\nu}Z^{\mu\nu} + \frac{1}{2}m_Z^2 Z_\mu Z^\mu - \frac{1}{2\xi}(\partial_\mu Z^\mu)^2 - \frac{1}{4}F_{\mu\nu}F^{\mu\nu} - \frac{1}{2\xi}(\partial_\mu A^\mu)^2\end{aligned}\quad (\text{A3})$$

where $F_{\mu\nu} = \partial_\mu A_\nu - \partial_\nu A_\mu$, $Z_{\mu\nu} = \partial_\mu Z_\nu - \partial_\nu Z_\mu$. Notice that, apart from the gauge fixing term $\partial_\mu A^\mu$, this lagrangian is $U_{\text{em}}(1)$ invariant.

On the other hand, the ghost sector is substantially modified in the non-linear gauge; however, since the gauge-fixing functionals are $U(1)$ invariant, the charged part of this sector is also invariant. We present now the corresponding Fadeev-Popov lagrangian, written in such a way that $U_{\text{em}}(1)$ invariance is explicit, namely:

$$\begin{aligned}\mathcal{L}_{\text{FPG}} = & -\bar{c}^- \left[\bar{D}_\mu \hat{D}^\mu + \xi m_W (m_W + \phi^0 + iG^0) \right] c^+ \\ & -igc_W \bar{c}^- \bar{D}_\mu (c_Z W^{+\mu}) - ie\bar{c}^- \bar{D}_\mu (c_\gamma W^{+\mu}) \\ & -i\frac{gs_W^2}{c_W} W^{+\mu} \bar{c}^- (\partial_\mu c_Z) + ieW^{+\mu} \bar{c}^- (\partial_\mu c_\gamma) \\ & -igc_W W^{+\mu} (\partial_\mu \bar{c}_Z) c^- - ieW^{+\mu} (\partial_\mu \bar{c}_\gamma) c^- \\ & -gc_{2w}\xi m_Z G^+ (\bar{c}^- c_Z + \bar{c}_Z c^-) - e\xi m_W G^+ (\bar{c}^- c_\gamma + \bar{c}_\gamma c^-) + h.c. \\ & -\bar{c}_Z [\square + \xi m_Z (m_Z + \phi^0)] c_Z - \bar{c}_\gamma \square c_\gamma\end{aligned}\quad (\text{A4})$$

where $c^\pm(\bar{c}^\pm)$, $c_Z(\bar{c}_Z)$, $c_\gamma(\bar{c}_\gamma)$ denote the pairs of ghosts associated with the W, Z, A gauge bosons respectively. The phase-convention for the charged ghost is $(c^+)^\dagger = c^-$ and $(\bar{c}^\dagger)^\dagger = \bar{c}^-$. In addition, one has: $\phi^0 = \cos(\alpha - \beta)H^0 + \sin(\alpha - \beta)h^0$, where h^0, H^0 denote the light and heavy neutral Higgs bosons of the MSSM. Notice that neither the charged Higgs (H^\pm) nor the CP-odd Higgs bosons (A^0) appear in this lagrangian, which can be understood if one reminds that these fields do not appear in the definition of the gauge fixing terms, and also because they do not receive a v.e.v..

Finally, we would like to mention the properties of the couplings of gauge bosons with the higgs and goldstone bosons. First, in this gauge the couplings $W^+G^-\gamma$ and W^+G^-Z are absent by construction, whereas the couplings $G^+G^-Z(\gamma)$, $H^+H^-Z(\gamma)$, $\phi^0W^+W^-$ and $W^+H^-\phi^0$ do not depend on the gauge-fixing procedure. However, the couplings $\phi^0G^+G^-$ or $\phi^0c^+c^-$ can depend on the choice of the gauge-fixing terms, when both the vector and scalars sectors are chosen non-linearly.

In conclusion, the Feynman rules needed for our calculation, which are depending of the gauge fixing procedure, arise from the lagrangians of Eqs. (A3-A4) written above.

APPENDIX B: LOOP FUNCTIONS ASSOCIATED TO NEUTRAL SCALARS

In this appendix we present the various loop functions coming from the $e^-\gamma \rightarrow e^-\phi^0$ processes. The functions arising from fermion, scalar and gauge boson loops, which characterize the $\phi^0\gamma^*\gamma$ and $\phi^0Z^*\gamma$ couplings, are given by:

$$\begin{aligned}F_f^{1/2} = & \frac{4m_f^2}{m_\phi^2 - t} \left\{ 1 - \frac{1}{2}(m_\phi^2 - t - 4m_f^2) C_0(t, m_\phi^2, m_f^2) \right. \\ & \left. + \frac{t}{m_\phi^2 - t} [B_0(m_\phi^2, m_f^2) - B_0(t, m_f^2)] \right\},\end{aligned}\quad (\text{B1})$$

$$F^0 = -\frac{4m_W^2}{m_\phi^2 - t} \left\{ 1 + 2m_{H^\pm}^2 C_0(t, m_\phi^2, m_{H^\pm}^2) + \frac{t}{m_\phi^2 - t} [B_0(m_\phi^2, m_{H^\pm}^2) - B_0(t, m_{H^\pm}^2)] \right\},\quad (\text{B2})$$

$$F_\gamma^1 = -\frac{4m_W^2}{m_\phi^2 - t} \left\{ 3 + \frac{m_\phi^2}{2m_W^2} + \left[3 \left(1 - \frac{m_\phi^2}{2m_W^2} \right) + \frac{2t}{m_W^2} \right] 2m_W^2 C_0(t, m_\phi^2, m_W^2) \right. \\ \left. + \left(3 + \frac{m_\phi^2}{2m_W^2} \right) \left(\frac{t}{m_\phi^2 - t} \right) [B_0(m_\phi^2, m_W^2) - B_0(t, m_W^2)] \right\}, \quad (\text{B3})$$

$$F_Z^1 = -4(3 - t_w^2) m_W^2 C_0(t, m_\phi^2, m_W^2) + \frac{2m_W^2}{m_\phi^2 - t} \left[5 + \frac{m_\phi^2}{2m_W^2} - \left(1 + \frac{m_\phi^2}{2m_W^2} \right) t_w^2 \right] \\ \times \left\{ 1 + 2m_W^2 C_0(t, m_\phi^2, m_W^2) + \frac{t}{m_\phi^2 - t} [B_0(m_\phi^2, m_W^2) - B_0(t, m_W^2)] \right\}, \quad (\text{B4})$$

where $C_0(t, m_\phi^2, m_i^2) = C_0(0, t, m_\phi^2, m_i^2, m_i^2, m_i^2)$, $B_0(m_\phi^2, m_i^2) = B_0(m_\phi^2, m_i^2, m_i^2)$ and $B_0(t, m_i^2) = B_0(t, m_i^2, m_i^2)$ are Passarino-Veltman three- and two-point scalar functions written in the notation of the FeynCalc program.

The loop functions coming from Z -mediated box diagram, including the related $\phi^0 e^{*-} e^-$ triangle graphs, are given by:

$$A(t, s, u) = \frac{1}{2st} \left\{ \frac{s - m_Z^2}{s} [m_Z^2(s + u) - su] D_0(1, 2, 3, 4) + (s - m_Z^2) [C_0(1, 2, 4) \right. \\ \left. + \frac{u}{s} C_0(1, 2, 3) - \frac{t + u}{s} C_0(2, 3, 4) + \frac{1}{s} \left(t - s - \frac{2m_Z^2 st}{(s + t)(s - m_Z^2)} \right) C_0(1, 3, 4) \right] \\ \left. + \frac{2t}{s + t} [B_0(3, 4) - B_0(1, 3)] \right\}. \quad (\text{B5})$$

$A(t, u, s)$ is obtained from $A(t, s, u)$ by means of the interchange $s \leftrightarrow u$. The arguments of the scalar functions are given by:

$$D_0(1, 2, 3, 4) = D_0(0, s, m_\phi^2, u, 0, 0, m_e^2, m_e^2, m_Z^2, m_Z^2), \\ C_0(1, 2, 4) = C_0(0, s, 0, m_e^2, m_e^2, m_Z^2), \\ C_0(1, 2, 3) = C_0(0, 0, u, m_e^2, m_e^2, m_Z^2), \\ C_0(2, 3, 4) = C_0(s, 0, m_\phi^2, m_Z^2, m_e^2, m_Z^2), \\ C_0(1, 3, 4) = C_0(0, m_\phi^2, u, m_e^2, m_Z^2, m_Z^2), \\ B_0(3, 4) = B_0(m_\phi^2, m_Z^2, m_Z^2), \\ B_0(1, 3) = B_0(u, m_e^2, m_Z^2). \quad (\text{B6})$$

Finally, the loop functions associated to the W -mediated box diagrams and its related triangle graphs are the following:

$$A_{12}(t, s, u) = 2c_w^4 [A_1(t, s, u) + A_2(t, u, s)], \\ A_{21}(t, s, u) = 2c_w^4 [A_2(t, s, u) + A_1(t, u, s)], \quad (\text{B7})$$

with

$$A_1(t, s, u) = \frac{1}{2st} \left\{ \frac{s - m_W^2}{s} [m_W^2(s + u) + st] D_0(1, 2, 3, 4) \right. \\ \left. + (s - m_W^2) \left[C_0(2, 3, 4) - \frac{t}{s} C_0(1, 3, 4) - \frac{s + u}{s} C_0(1, 2, 3) \right. \right. \\ \left. \left. + \frac{u + t}{s} C_0(1, 2, 4) \right] + \frac{2t}{s + u} [B_0(1, 2) - B_0(1, 3)] \right\}, \quad (\text{B8})$$

$$A_2(t, s, u) = \frac{1}{2tu} \left\{ \left[\frac{t + u - m_W^2}{u} (m_W^2(s + u) - st) - 2m_W^2 t \right] D_0(1, 2, 3, 4) \right.$$

$$\begin{aligned}
& + (t + u - m_W^2) \left[\frac{s}{u} C_0(2, 3, 4) + \frac{t}{u} C_0(1, 3, 4) \right. \\
& - \frac{s + u}{u} C_0(1, 2, 3) + \frac{u^2 - 2ut - t^2}{u(t + u)} C_0(1, 2, 4) \left. \right] \\
& + \frac{2t}{t + u} [B_0(2, 4) - B_0(1, 2)] + \frac{2t}{s + u} [B_0(1, 3) - B_0(1, 2)] \Big\}. \tag{B9}
\end{aligned}$$

The scalar functions have the following arguments:

$$\begin{aligned}
D_0(1, 2, 3, 4) &= D_0(0, 0, 0, m_\phi^2, t, s, m_W^2, 0, m_W^2, m_W^2), \\
C_0(2, 3, 4) &= C_0(0, 0, s, 0, m_W^2, m_W^2), \\
C_0(1, 3, 4) &= C_0(0, 0, t, m_W^2, 0, m_W^2), \\
C_0(1, 2, 3) &= C_0(t, 0, m_\phi^2, m_W^2, m_W^2, m_W^2), \\
C_0(1, 2, 4) &= C_0(0, s, m_\phi^2, m_W^2, 0, m_W^2), \\
B_0(1, 2) &= B_0(m_\phi^2, m_W^2, m_W^2), \\
B_0(1, 3) &= B_0(t, m_W^2, m_W^2), \\
B_0(2, 4) &= B_0(s, 0, m_W^2). \tag{B10}
\end{aligned}$$

The expressions for $A_1(t, u, s)$ and $A_2(t, u, s)$ can be obtained from the respective $A_1(t, s, u)$ and $A_2(t, s, u)$ through the interchange $s \leftrightarrow u$.

APPENDIX C: LOOP FUNCTIONS ASSOCIATED TO CHARGED SCALARS

In this appendix we shall write the explicit formulae for the functions V_f , $V_{H^\pm \phi^0}$, $V_{W\phi^0}$ and A_f using a notation that, hopefully, facilitates its use by the interested reader. Our convention for the scalar functions B_0 , C_0 is the same as in the previous Appendix. In this case, the contributions arising from loops with fermions, scalars and gauge bosons, have the following expression:

$$\begin{aligned}
V_f &= \sum_f \frac{N_c}{t - m_{H^\pm}^2} \{ (Q_u + Q_d) (m_d^2 \tan \beta + m_u^2 \cot \beta) \\
& + 2Q_d [m_d^2 (m_d^2 \tan \beta + m_u^2 \cot \beta) - (t - m_{H^\pm}^2) m_d^2 \tan \beta] C_0(0, m_{H^\pm}^2, t, m_d^2, m_d^2, m_u^2) \\
& + 2Q_u [m_u^2 (m_d^2 \tan \beta + m_u^2 \cot \beta) - (t - m_{H^\pm}^2) m_u^2 \cot \beta] C_0(0, m_{H^\pm}^2, t, m_u^2, m_u^2, m_d^2) \\
& + \left[\frac{m_d^2 \tan \beta + m_u^2 \cot \beta}{t - m_{H^\pm}^2} (m_u^2 - m_d^2 + (Q_u + Q_d) m_{H^\pm}^2) \right. \\
& + 2(Q_d m_d^2 \tan \beta + Q_u m_u^2 \cot \beta) [B_0(t, m_d^2, m_u^2) - B_0(m_{H^\pm}^2, m_d^2, m_u^2)] \\
& \left. + m_u m_d \frac{m_u^2 - m_d^2}{m_{H^\pm}^2} [B_0(m_{H^\pm}^2, m_d^2, m_u^2) - B_0(0, m_d^2, m_u^2)] \right\}, \tag{C1}
\end{aligned}$$

and

$$\begin{aligned}
A_f &= \sum_f N_c \{ Q_d m_d^2 \tan \beta C_0(0, m_{H^\pm}^2, t, m_d^2, m_d^2, m_u^2) - Q_u m_u^2 \cot \beta C_0(0, m_{H^\pm}^2, t, m_u^2, m_u^2, m_d^2) \\
& + \frac{m_d^2 \tan \beta + m_u^2 \cot \beta}{t - m_{H^\pm}^2} [B_0(t, m_d^2, m_u^2) - B_0(m_{H^\pm}^2, m_d^2, m_u^2)] \Big\}, \tag{C2}
\end{aligned}$$

$$\begin{aligned}
V_{H^+ \phi^0} &= \sum_{\phi^0 = h^0, H^0} (-v_{\phi^0} s_{\phi^0}) \frac{m_W^2}{t - m_{H^\pm}^2} \{ 1 + 2m_{H^\pm}^2 C_0(0, t, m_{H^\pm}^2, m_{H^\pm}^2, m_{H^\pm}^2, m_{\phi^0}^2) \\
& + \left(\frac{m_{\phi^0}^2 - m_{H^\pm}^2 - t}{t - m_{H^\pm}^2} \right) [B_0(t, m_{H^\pm}^2, m_{\phi^0}^2) - B_0(m_{H^\pm}^2, m_{H^\pm}^2, m_{\phi^0}^2)] \\
& + \left(\frac{m_{\phi^0}^2 - m_{H^\pm}^2}{m_{H^\pm}^2} \right) [B_0(0, m_{H^\pm}^2, m_{\phi^0}^2) - B_0(m_{H^\pm}^2, m_{H^\pm}^2, m_{\phi^0}^2)] \Big\}, \tag{C3}
\end{aligned}$$

$$\begin{aligned}
V_{W\phi^0} = & \sum_{\phi^0=h^0, H^0} (-\sigma_{\phi^0} v_{\phi^0}) \frac{m_W^2}{t - m_{H^\pm}^2} \left\{ \frac{m_{H^\pm}^2 - m_{\phi^0}^2 + m_W^2}{2m_W^2} \right. \\
& + (3m_{H^\pm}^2 - m_{\phi^0}^2 + m_W^2 - 2t) C_0(0, m_{H^\pm}^2, t, m_W^2, m_W^2, m_{\phi^0}^2) \\
& + \frac{(m_{H^\pm}^2 - m_{\phi^0}^2 - m_W^2)(m_{\phi^0}^2 - m_W^2 - t) - 4m_W^2(m_{H^\pm}^2 - t)}{2m_W^2(t - m_{H^\pm}^2)} \\
& \times [B_0(t, m_W^2, m_W^2) - B_0(m_{H^\pm}^2, m_W^2, m_W^2)] \\
& \left. + \frac{(m_{\phi^0}^2 - m_W^2)(m_{H^\pm}^2 - m_{\phi^0}^2 + m_W^2)}{2m_W^2 m_{H^\pm}^2} [B_0(0, m_W^2, m_{\phi^0}^2) - B_0(m_{H^\pm}^2, m_W^2, m_{\phi^0}^2)] \right\}, \quad (C4)
\end{aligned}$$

where $\sigma_{H^0} = -v_{h^0}$, $\sigma_{h^0} = -v_{H^0}$ and $\phi_1^0 = H^0$, $\phi_2^0 = h^0$.

-
- [1] J. F. Gunion, H. E. Haber, G. Kane, and S. Dawson, *The Higgs hunter's guide*. No. 80 in Frontiers in Physics. Addison-Wesley, Reading MA, USA, 2 ed., 1990.
 - [2] S. P. Martin, "A Supersymmetry primer. In Kane, G.L. (ed.): Perspectives on supersymmetry 1-98.," **hep-ph/9709356**.
 - [3] Y. Okada, M. Yamaguchi, and T. Yanagida, "Upper bound of the lightest Higgs boson mass in the minimal supersymmetric standard model," *Prog. Theor. Phys.* **85** (1991) 1-6.
 - [4] H. E. Haber and R. Hempfling, "Can the mass of the lightest Higgs boson of the minimal supersymmetric model be larger than m_Z ?," *Phys. Rev. Lett.* **66** (1991) 1815-1818.
 - [5] J. Ellis, G. Ridolfi, and F. Zwirner, "Radiative corrections to the masses of supersymmetric Higgs bosons," *Phys. Lett.* **B257** (1991) 83-91.
 - [6] Z. Kunszt and F. Zwirner, "Testing the Higgs sector of the minimal supersymmetric standard model at large hadron colliders," *Nucl. Phys.* **B385** (1992) 3-75, **hep-ph/9203223**.
 - [7] R.-J. Zhang, "Two loop effective potential calculation of the lightest CP even Higgs boson mass in the MSSM," *Phys. Lett.* **B447** (1999) 89, **hep-ph/9808299**.
 - [8] S. Heinemeyer, W. Hollik, and G. Weiglein, "QCD corrections to the masses of the neutral CP - even Higgs bosons in the MSSM," *Phys. Rev.* **D58** (1998) 091701, **hep-ph/9803277**.
 - [9] **ALEPH** Collaboration, M. P. Altarelli, "Higgs searches and prospects from LEP-2," **hep-ex/9904006**.
 - [10] J. Ellis, "Theoretical summary: 1999 Electroweak Session of the Rencontres de Moriond," **hep-ph/9906229**.
 - [11] M. Carena, S. Mrenna, and C. E. M. Wagner, "MSSM Higgs boson phenomenology at the Tevatron collider," **hep-ph/9808312**.
 - [12] J. Dai, J. F. Gunion, and R. Vega, "Detection of neutral MSSM Higgs bosons in four b final states at the Tevatron and the LHC: An update," *Phys. Lett.* **B387** (1996) 801-803, **hep-ph/9607379**.
 - [13] C. Balazs, J. L. Diaz-Cruz, H. J. He, T. Tait, and C. P. Yuan, "Probing Higgs bosons with large bottom Yukawa coupling at hadron colliders," *Phys. Rev.* **D59** (1999) 055016, **hep-ph/9807349**.
 - [14] M. Spira, "QCD effects in Higgs physics," *Fortsch. Phys.* **46** (1998) 203, **hep-ph/9705337**.
 - [15] J. F. Gunion and L. H. Orr, "Detecting the Higgs bosons of the minimal supersymmetric model," *Phys. Rev.* **D46** (1992) 2052-2067.
 - [16] J. L. Diaz-Cruz and O. A. Sampayo, "Detection of SUSY Higgs bosons after radiative corrections," *Int. J. Mod. Phys.* **A8** (1993) 4339-4354.
 - [17] M. Dittmar and H. Dreiner, "How to find a Higgs boson with a mass between 155-GeV - 180-GeV at the LHC," *Phys. Rev.* **D55** (1997) 167-172, **hep-ph/9608317**.
 - [18] T. Plehn, D. Rainwater, and D. Zeppenfeld, "Probing the MSSM Higgs sector via weak boson fusion at the LHC," *Phys. Lett.* **B454** (1999) 297, **hep-ph/9902434**.
 - [19] **NLC ZDR Design Group and NLC Physics Working Group** Collaboration, S. Kuhlman *et. al.*, "Physics and technology of the Next Linear Collider: A Report submitted to Snowmass '96," **hep-ex/9605011**.
 - [20] **ECFA/DESY LC Physics Working Group** Collaboration, E. Accomando *et. al.*, "Physics with e+ e- linear colliders," *Phys. Rept.* **299** (1998) 1, **hep-ph/9705442**.
 - [21] T. Tsuchi, "Physics plan at JLC,". Invited talk at International Conference on Hadron Structure (HS 98), Stara Lesna, Slovakia, 7-13 Sep 1998.
 - [22] H. E. Haber *et. al.*, "Weakly coupled Higgs bosons and precision electroweak physics," **hep-ph/9703391**.

- [23] A. Barroso, J. Pulido, and J. C. Romao, “Higgs production at e^+e^- colliders,” *Nucl. Phys.* **B267** (1986) 509–530.
- [24] S. Komamiya, “Searching for charged higgs bosons at $O(\frac{1}{2})$ TeV to 1 TeV e^+e^- colliders,” *Phys. Rev.* **D38** (1988) 2158.
- [25] G. Giacomelli and P. Giacomelli, “Particle searches at LEP,” *Riv. Nuovo Cim.* **16** (1993) 1–58.
- [26] O. J. P. Eboli, M. C. Gonzalez-Garcia, F. Halzen, and D. Zeppenfeld, “Measuring the gamma gamma coupling of the Higgs at linear colliders,” *Phys. Rev.* **D48** (1993) 1430–1432, [hep-ph/9302284](#).
- [27] J. M. Hernandez, M. A. Perez, and J. J. Toscano, “New physics effects on Higgs production at gamma gamma colliders,” *Phys. Lett.* **B375** (1996) 227, [hep-ph/9601378](#).
- [28] U. Cotti, J. L. Diaz-Cruz, and J. J. Toscano, “Exact formulae for Higgs production through $e\gamma \rightarrow eH$ in the nonlinear R_ξ gauge,” *Phys. Lett.* **B404** (1997) 308–314, [hep-ph/9704304](#).
- [29] E. Gabrielli, V. A. Ilin, and B. Mele, “Z gamma H vertex effects in Higgs production at future e gamma linear colliders,” *Phys. Rev.* **D56** (1997) 5945–5961, **Erratum-ibid.** **D58:119902**, 1998 [hep-ph/9702414](#).
- [30] Y. Liao and W. W. Repko, “Production of neutral scalar Higgs bosons at e gamma colliders,” *Phys. Rev.* **D57** (1998) 6998–7005, [hep-ph/9711202](#).
- [31] D. A. Dicus and W. W. Repko, “Production of pseudoscalar Higgs bosons in e gamma collisions,” *Phys. Rev.* **D53** (1996) 3616–3619, [hep-ph/9601297](#).
- [32] A. T. Banin, I. F. Ginzburg, and I. P. Ivanov, “Anomalous interactions in Higgs boson production at photon colliders,” *Phys. Rev.* **D59** (1999) 115001, [hep-ph/9806515](#).
- [33] E. Gabrielli, V. A. Ilyin, and B. Mele, “Looking for anomalous gamma-gamma H and Z gamma H couplings at future linear collider,” [hep-ph/9902362](#).
- [34] A. Dobado, M. J. Herrero, and S. Penaranda, “Do heavy sfermions decouple from low-energy standard model?,” [hep-ph/9806488](#).
- [35] R. Barbieri and M. Frigeni, “The Supersymmetric Higgs searches at LEP after radiative corrections,” *Phys. Lett.* **B258** (1991) 395–398.
- [36] R. Mertig, M. Bohm, and A. Denner, “FEYN CALC: Computer algebraic calculation of Feynman amplitudes,” *Comput. Phys. Commun.* **64** (1991) 345.
- [37] G. J. van Oldenborgh, “FF: A Package to evaluate one loop Feynman diagrams,” *Comput. Phys. Commun.* **66** (1991) 1.
- [38] G. J. van Oldenborgh and J. A. M. Vermaseren, “New algorithms for one loop integrals,” *Z. Phys.* **C46** (1990) 425–438.
- [39] C. Caso *et. al.*, “Review of particle physics. Particle Data Group,” *Eur. Phys. J.* **C3** (1998) 1–794.
- [40] M. Spira, A. Djouadi, D. Graudenz, and P. M. Zerwas, “Higgs boson production at the LHC,” *Nucl. Phys.* **B453** (1995) 17–82, [hep-ph/9504378](#).
- [41] E. E. Boos, M. N. Dubinin, V. A. Ilin, A. E. Pukhov, and V. I. Savrin, “CompHEP: Specialized package for automatic calculations of elementary particle decays and collisions,” [hep-ph/9503280](#).
- [42] P. A. Baikov *et. al.*, “Physical results by means of CompHEP,” [hep-ph/9701412](#).
- [43] D. Bowser-Chao, K. Cheung, and S. Thomas, “Detecting an intermediate mass charged Higgs at gamma gamma colliders,” *Phys. Lett.* **B315** (1993) 399–405, [hep-ph/9304290](#).
- [44] E. Boos, A. Pukhov, M. Sachwitz, and H. J. Schreiber, “Probing anomalous W t b coupling via single top production at TeV energy gamma e colliders,” *Phys. Lett.* **B404** (1997) 119–123, [hep-ph/9704259](#).
- [45] K. Fujikawa, B. W. Lee, and A. I. Sanda, “Generalized renormalizable gauge formulation of spontaneously broken gauge theories,” *Phys. Rev.* **D6** (1972) 2923.
- [46] M. Bace and N. D. H. Dass, “Parity violating compton amplitude in unified theories,” *Ann. Phys.* **94** (1975) 349.
- [47] M. B. Gavela, G. Girardi, C. Malleville, and P. Sorba, “A nonlinear R_ξ gauge condition for the electroweak $SU(2)\times U(1)$ model,” *Nucl. Phys.* **B193** (1981) 257.
- [48] N. G. Deshpande and M. Nazerimonfared, “Flavor changing electromagnetic vertex in a nonlinear R_ξ gauge,” *Nucl. Phys.* **B213** (1983) 390.
- [49] J. M. Hernandez, M. A. Perez, G. Tavares-Velasco, and J. J. Toscano, “The Decay $Z \rightarrow \text{neutrino anti-neutrino photon}$ in the Standard Model,” [hep-ph/9903391](#).

FIG. 1. Classification of graphs that contributes to the reaction $e\gamma \rightarrow eh^0$.

FIG. 2. Total cross section for the reaction $e\gamma \rightarrow eh^0$ for different values of $\tan\beta$, with $\sqrt{s} = 500$ GeV.

FIG. 3. Total cross section for the reaction $e\gamma \rightarrow eH^0$ for different values of $\tan\beta$, with $\sqrt{s} = 500$ GeV.

FIG. 4. Total cross section for the reaction $e\gamma \rightarrow eA^0$ for different values of $\tan\beta$, with $\sqrt{s} = 500$ GeV.

FIG. 5. Cross section contour lines for the reaction $e\gamma \rightarrow eh^0$, for different values of $\sigma(\text{fb})$, with $\sqrt{s} = 500$ GeV. The region to the right from the heavy (dashed) line is where the signal is detectable (above backgrounds at the 3 (5) σ level).

FIG. 6. Cross section contour lines for the reaction $e\gamma \rightarrow eH^0$, for different values of $\sigma(\text{fb})$, with $\sqrt{s} = 500$ GeV. The region to the left from the heavy (dashed) line is where the signal is detectable (above backgrounds at the 3 (5) σ level).

FIG. 7. Cross section contour lines for the reaction $e\gamma \rightarrow eA^0$, for different values of $\sigma(\text{fb})$, with $\sqrt{s} = 500$ GeV.

FIG. 8. Classification of graphs that contributes to the reaction $e^-\gamma \rightarrow \nu_e H^-$.

FIG. 9. Cross section contour lines for the reaction $e^-\gamma \rightarrow \nu H^-$, for different values of $\tan\beta$, with $\sqrt{s} = 500$ GeV.

FIG. 10. Cross section for the reaction $e^-\gamma \rightarrow \nu H^-$, with $\sqrt{s} = 500$ GeV compared with different production channels.

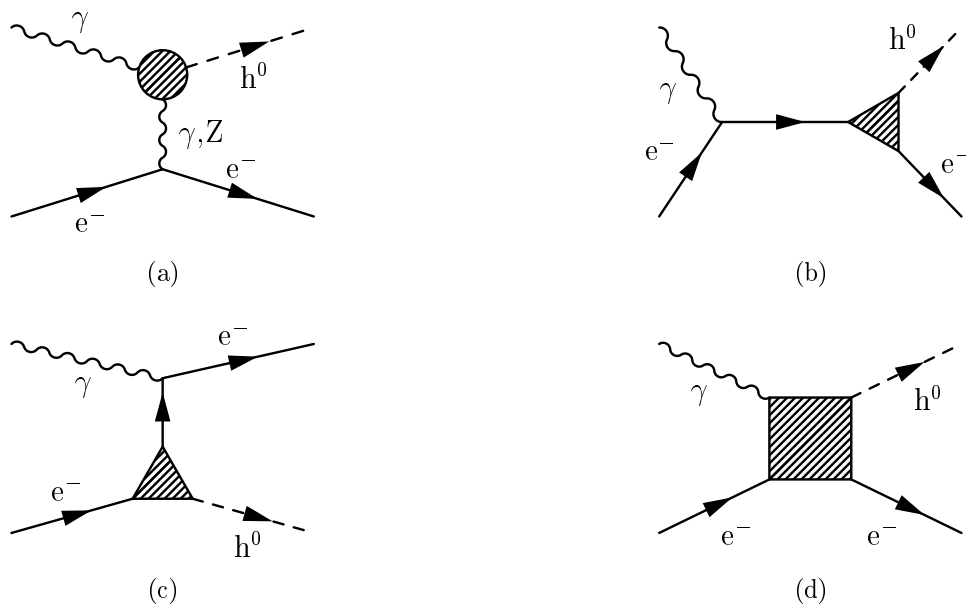


Figure 1

Figure 2

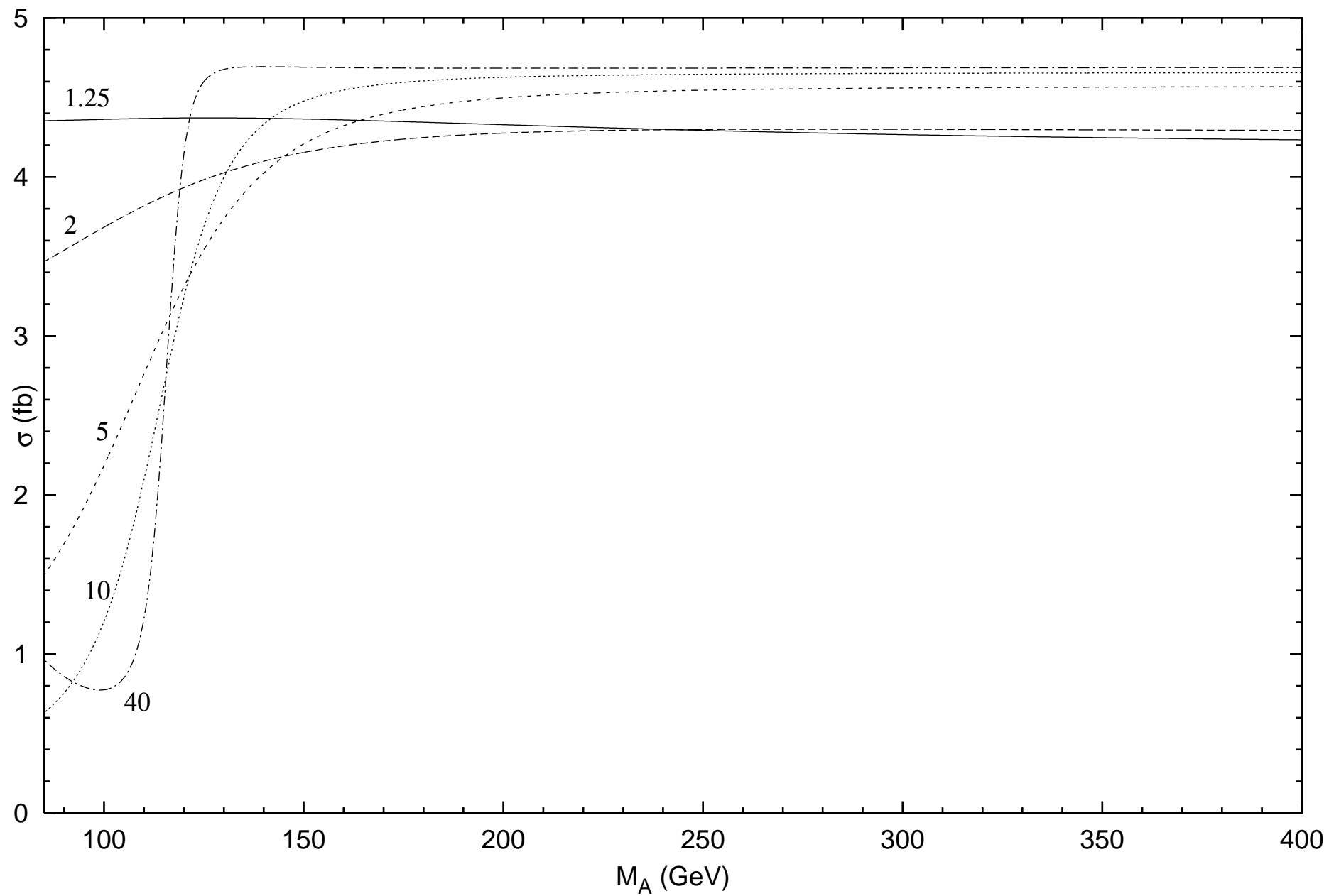


Figure 3

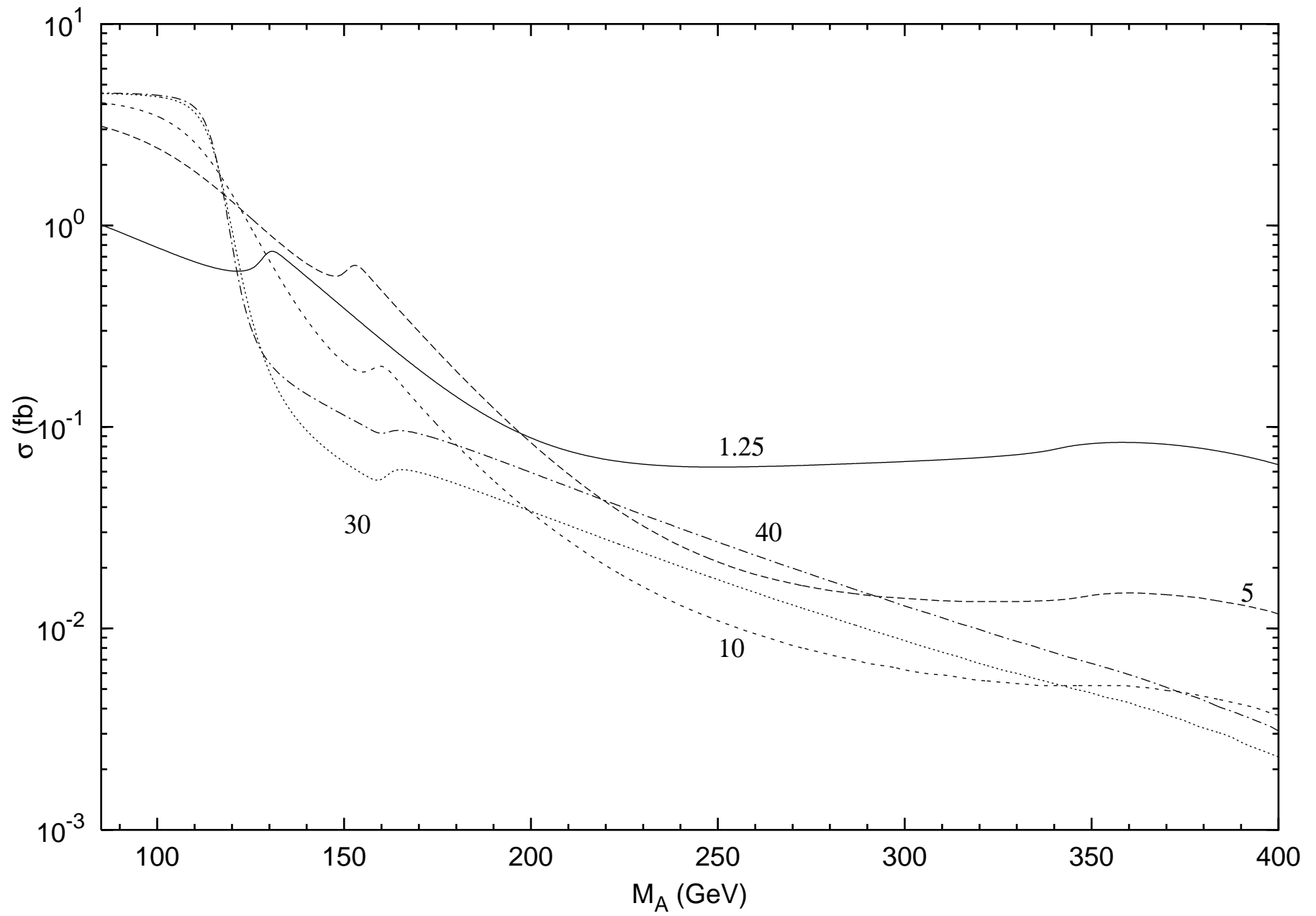


Figure 4

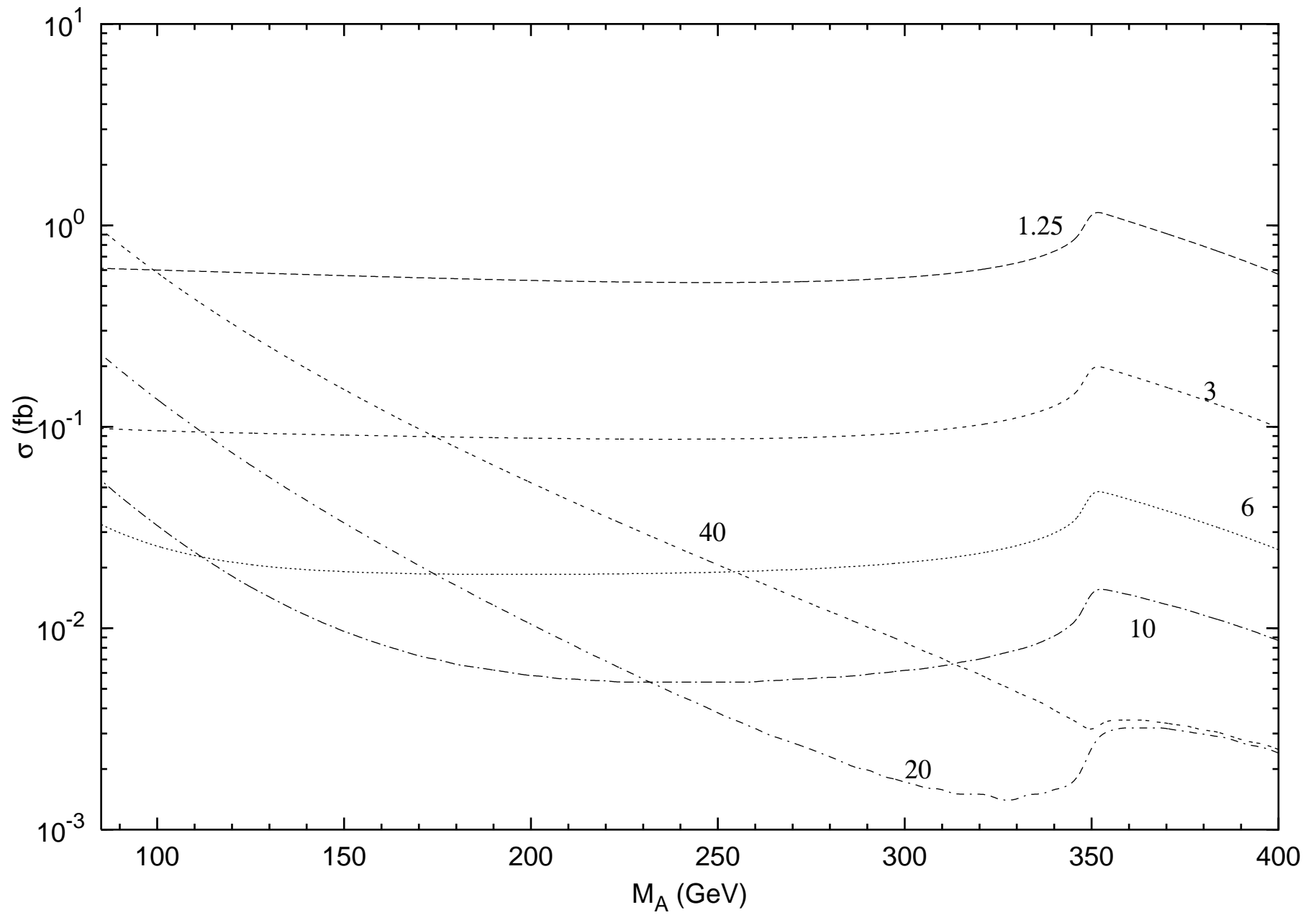


Figure 5

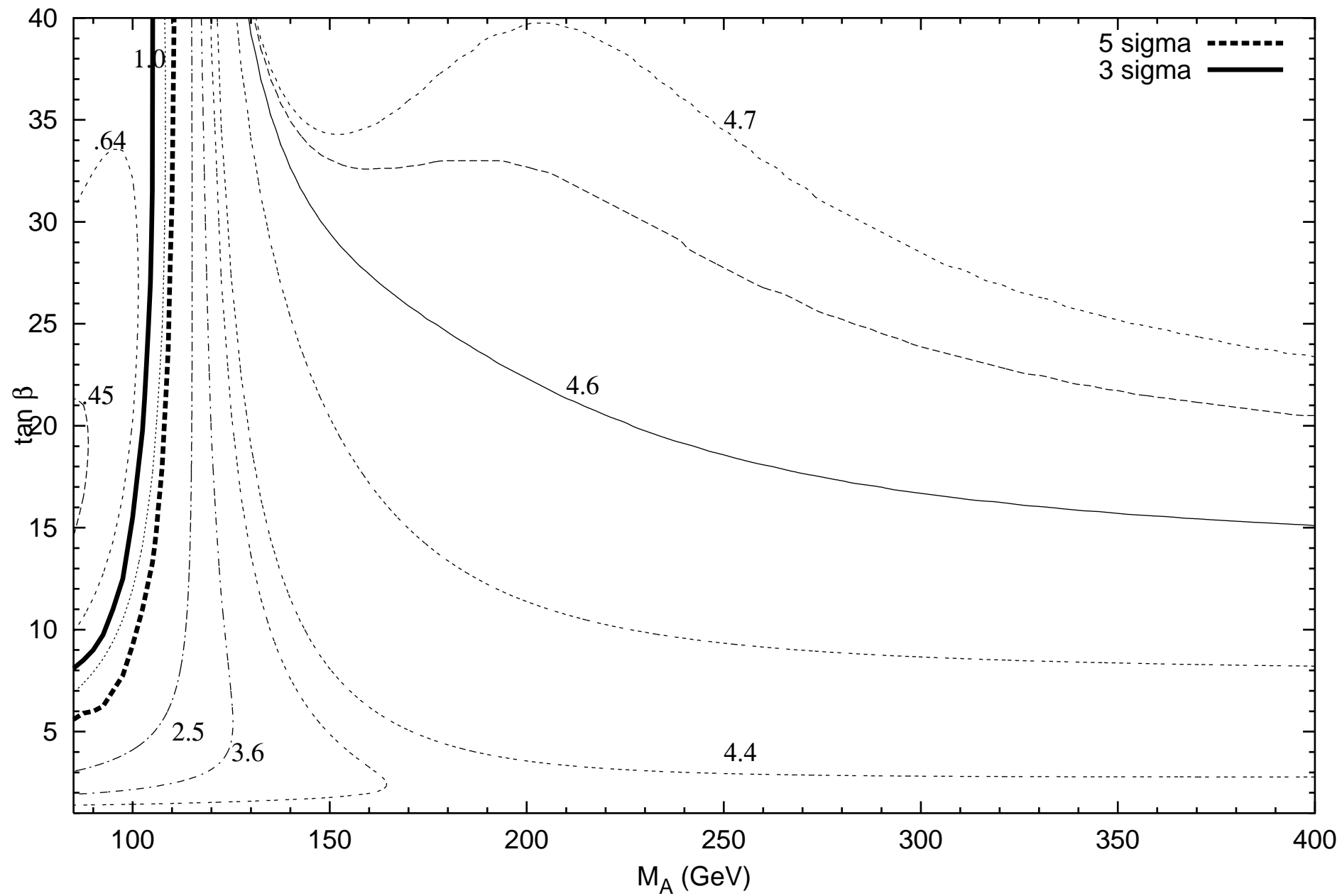


Figure 6

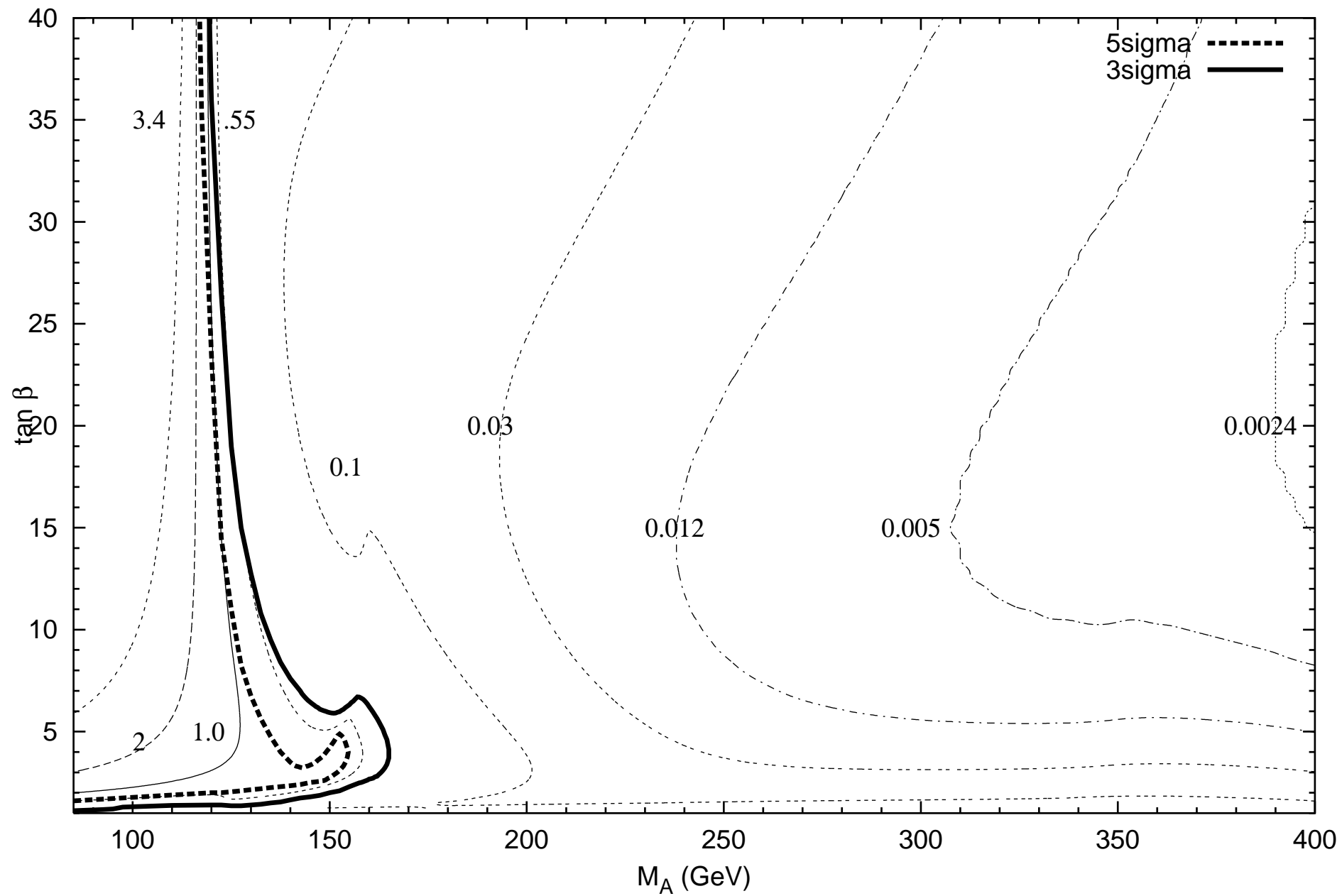
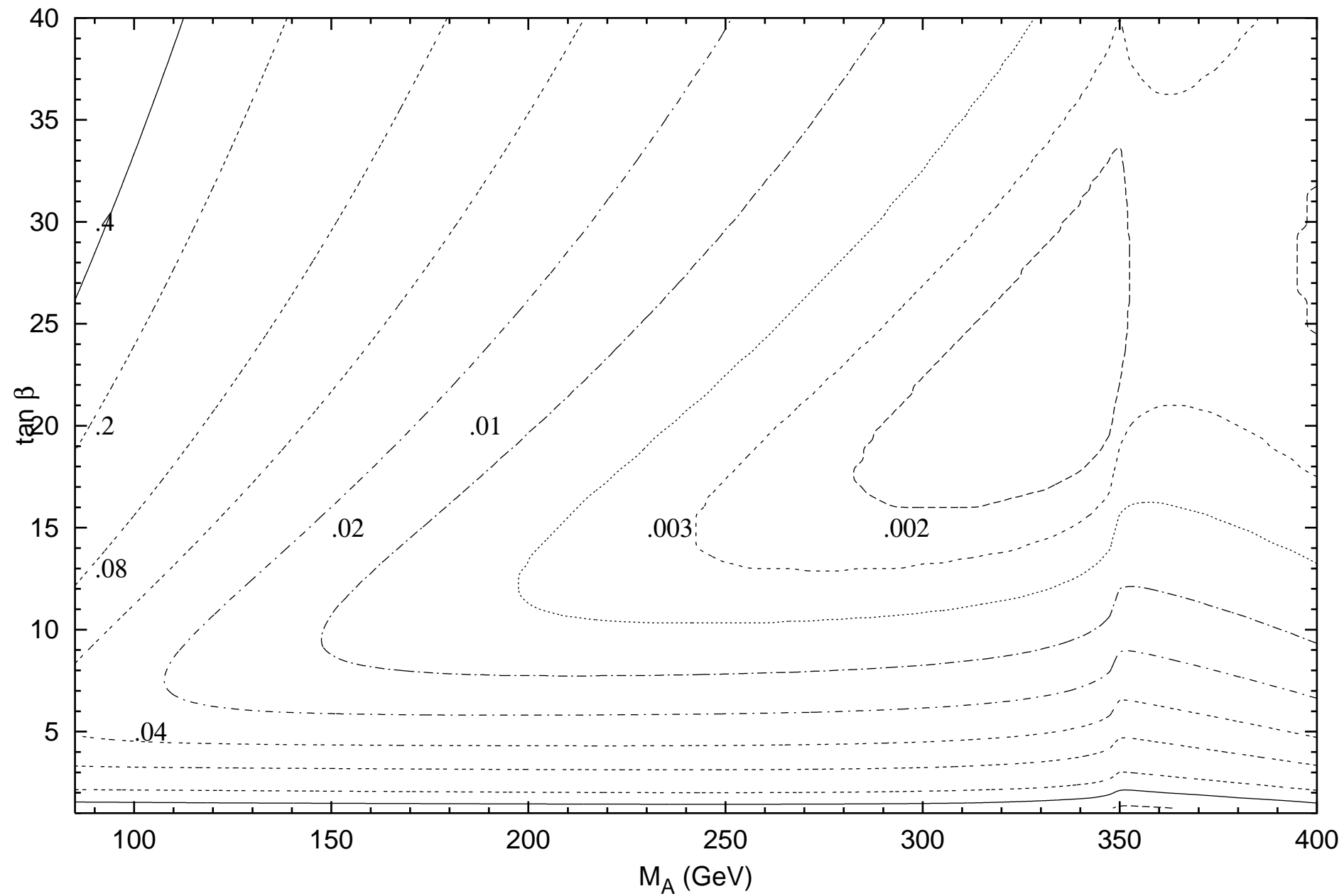


Figure 7



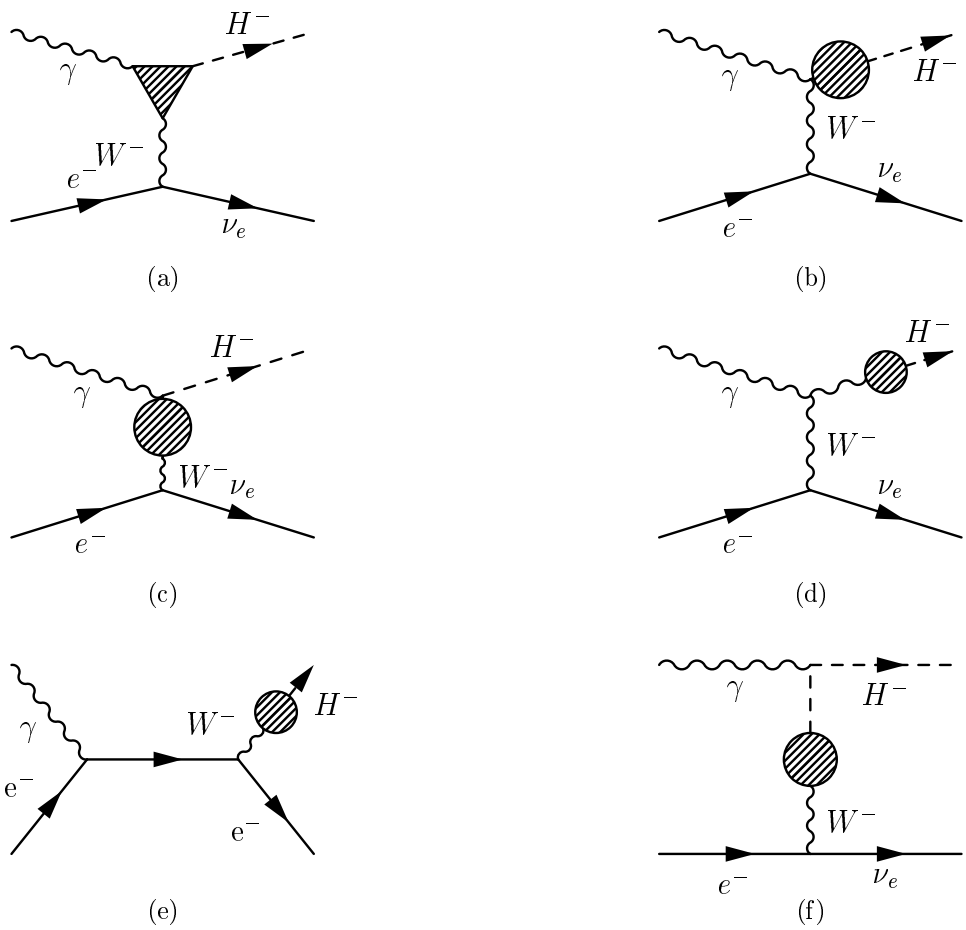


Figure 8

Figure 9

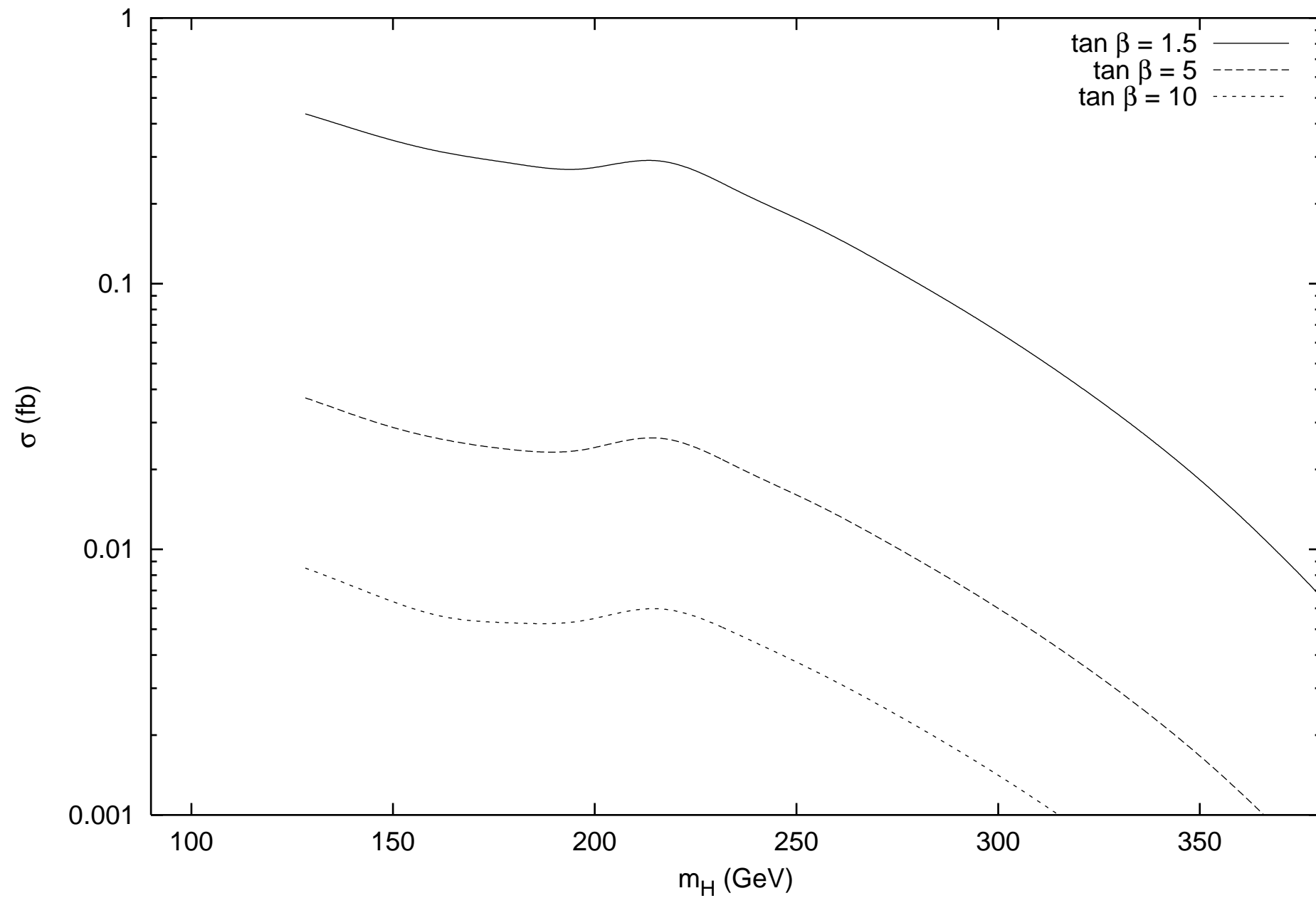


Figure 10

